

Article

Phytogenic Synthesis and Characterization of Silver Metallic/Bimetallic Nanoparticles Using *Beta vulgaris* L. Extract and Assessments of Their Potential Biological Activities

Khaled M. Elattar ^{1,*}, Abeer A. Ghoniem ², Fatimah O. Al-Otibi ³, Mohammed S. El-Hersh ², Yosra A. Helmy ⁴ 
and WesamEldin I. A. Saber ^{2,*} 

- ¹ Unit of Genetic Engineering and Biotechnology, Faculty of Science, Mansoura University, El-Gomhoria Street, Mansoura 35516, Egypt
- ² Microbial Activity Unit, Department of Microbiology, Soils, Water and Environment Research Institute, Agricultural Research Center, Giza 12619, Egypt; abeer.abdelkhalik@yahoo.com (A.A.G.); m.elhersh@yahoo.com (M.S.E.-H.)
- ³ Botany and Microbiology Department, Faculty of Science, King Saud University, Riyadh 11451, Saudi Arabia; falotibi@ksu.edu.sa
- ⁴ Department of Veterinary Science, Martin-Gatton College of Agriculture, Food, and Environment, University of Kentucky, Lexington, KY 40546, USA; yosra.helmy@uky.edu
- * Correspondence: khaledelattar2@yahoo.com (K.M.E.); wesameldin.saber@arc.sci.eg (W.I.A.S.)

Featured Application: The specific application of this work lies in the new avenue synthesis of nanomedicines—particularly Ag-mNPs, AgSeO₂-bmNPs, and Ag-TiO₂-bmNPs—using eco-friendly methods. These nanoparticles have shown significant potential as they can be used for potent antioxidant and antibacterial activities. The use of *Beta vulgaris* extract for the bio-reduction process adds to the environmentally sustainable aspect of the research. Furthermore, the antioxidant activity of the nanoparticles supports their potential medical applications beyond antibacterial therapy. Additionally, the study paves the way for future research into utilizing nature-inspired approaches for green and effective medical advancements.



Citation: Elattar, K.M.; Ghoniem, A.A.; Al-Otibi, F.O.; El-Hersh, M.S.; Helmy, Y.A.; Saber, W.I.A. Phytogenic Synthesis and Characterization of Silver Metallic/Bimetallic Nanoparticles Using *Beta vulgaris* L. Extract and Assessments of Their Potential Biological Activities. *Appl. Sci.* **2023**, *13*, 10110. <https://doi.org/10.3390/app131810110>

Academic Editor: Monica Gallo

Received: 3 August 2023

Revised: 30 August 2023

Accepted: 4 September 2023

Published: 8 September 2023



Copyright: © 2023 by the authors. Licensee MDPI, Basel, Switzerland. This article is an open access article distributed under the terms and conditions of the Creative Commons Attribution (CC BY) license (<https://creativecommons.org/licenses/by/4.0/>).

Abstract: The synthesis of novel nanomedicines through eco-friendly protocols has been applied on a large scale with the prediction of discovering alternate therapies. The current work attained phytogenic synthesis of Ag-mNPs, AgSeO₂-bmNPs, and Ag-TiO₂-bmNPs through bio-reduction using an aqueous extract of *Beta vulgaris* (red beetroot). The phytochemical profile of the eco-friendly synthesized metallic/bimetallic nanoparticles was studied. The optical properties of nano-solutions were studied via UV-visible spectroscopy. The Fourier-transform infrared spectroscopy (FT-IR) spectral analyses revealed that stretching vibrations at wavenumbers 3303.81–3327.81 cm⁻¹ attributed to phenolic hydroxyl groups documented shifts in the values in this range owing to proton dissociation through the bio-reduction of the metal ions. The surface morphology and the charge of the nanoparticles were investigated using a Transmission Electron Microscope (TEM) and zeta potential analyses. The prepared nano-solutions showed lower antioxidant activity (1,1-Diphenyl-2-picrylhydrazyl (DPPH•) and phosphomolybdate assays) than the plant extract. These results together with phytochemical analyses support the participation of the reactive species (phenolic contents) in the bio-reduction of the metal ions in the solutions through the formation of metallic/bimetallic nanoparticles. Ag-mNPs, AgSeO₂-bmNPs, and Ag-TiO₂-bmNPs showed antibacterial potentiality. AgSeO₂-bmNPs were superior with inhibitory zone diameters of 34.7, 37.7, 11.7, and 32.7 mm against *Enterococcus faecalis*, *Staphylococcus aureus*, *Escherichia coli*, and *Salmonella enterica*, respectively. Applying the Methylthiazole Tetrazolium (MTT) assay, the Ag-TiO₂ bmNPs revealed potent cytotoxicity against the HePG2 tumor cell line (IC₅₀ = 18.18 ± 1.5 µg/mL), while Ag-SeO₂ bmNPs revealed the most potent cytotoxicity against the MCF-7 cell line (IC₅₀ = 17.92 ± 1.4 µg/mL).

Keywords: human pathogenic bacteria; antioxidant activity; phytochemical; spectroscopic analyses; biological assessments

1. Introduction

Nowadays, the field of nanotechnology has been recognized as an attractive science, since nanoparticles (NPs) have varied applications in numerous areas, e.g., electric, chemical, biomedical branches, and other industrial applications. Subsequently, the global production of engineered nanoparticles is continuously increasing [1], wherein there are over 1800 consumer products containing engineered nanoparticles [2]. Furthermore, NPs play a crucial role in drug delivery, cosmetics industries, catalytic regions, antimicrobial/antiseptic uses, medical purposes, etc. [3,4]. The major NPs that are prevalent in consumer products involve silver (Ag mNPs), gold (Au mNPs), copper (Cu mNPs), palladium (Pd mNPs), titanium dioxide (TiO₂ mNPs), zinc oxide (ZnO mNPs), etc. [5].

However, there are growing concerns about the hazards of exposure to engineered nanoparticles, which cause environmental risks while penetrating numerous regions of the environment [6]. Moreover, engineered nanoparticles have adverse effects on human and ecological health [7]. With the exclusion of understanding the crucial criteria of chemical mechanisms of formation and the interaction of engineered nanoparticles, there are limited mitigation strategies available for avoiding concerns to human health.

Another type of nanoparticle is incidental nanoparticles (INPs), such as Magneli phases from natural TiO₂ minerals containing coal [8], and additionally, carbon black soot, consisting of either fullerene or graphene, is generated from the emissions of combustion [9]. These INPs have emerged as noteworthy environmental pollutants present in the atmosphere, water bodies, and soil [10]. Further, natural nanoparticles could also be formed via photochemical, biological, or extraterrestrial processes [11]. Several studies have attained the fate of NPs among environmental regions, where oxygen levels, pH, organic matter, ionic strength, and light conditions all influence the fate of NPs [12].

Generally, nanoparticles are created with distinct characteristics that render them highly sought after in the fields of materials science and biology [13]. Among the diverse array of nanoparticles, Ag-NPs have emerged as one of the most extensively researched subjects in recent decades [14]. Silver nanoparticles consist of a range of 20 to 15,000 silver atoms, typically possessing diameters smaller than 100 nm, owing to their significant surface-to-volume ratio. These Ag-NPs demonstrate notable antimicrobial efficacy, even when present in low concentrations [15]. Additionally, Ag-NPs are low-cost and have shown low cytotoxicity and immunological response [16]; so, Ag-NPs are currently used in numerous applications. The discharge of Ag-NPs into aquatic ecosystems, the dissociation into ions, the binding to organic matter, reactions with other metal-based materials, and disruption of normal biological and ecological processes at the cellular level are all possible negative effects of Ag-NP usage. The creation of natural Ag-NPs is substantially affected by various chemical factors such as pH, levels of oxygen, and the existence of organic substances [1]. This process leads to the development of Ag-NPs that possess long-term stability. Moreover, Ag-NPs can engage with both metal and metal oxide particles/nanoparticles. However, there exists limited information regarding the chemical and toxicological connections between Ag-NPs and other types of nanoparticles. The interaction of Ag-NPs with gold nanoparticles and titanium dioxide nanoparticles has been investigated and discussed [1].

The synthesis of Ag-NPs could be construed during physical, chemical, and biological procedures [17], where their synthesis formed in different sizes, ranging from 1 to 100 nm. The chemical and physical procedures were used to create nanoparticles; however, the chemical procedures used substances during the reduction process of metallic ions. This, in turn, has some disadvantageous traits, including chemical toxins and some precarious compounds in their products [18]. The size of NPs could be influenced by pH, temperature, and metal concentrations [19]. Otherwise, the biological approaches have the merit of simplicity in NP synthesis, less time of reaction, low toxicity and cost, high yield, and biocompatibility, which are critical and imperative.

The biosynthesis of Ag-NPs concerning plant extracts was conducted, in which Ag-NPs were synthesized using different plant extracts e.g., Lucerne, Pine, Persimmon, Mag-

nia, Platanus, apple, pineapple, and Ginkgo [20–23]. Likewise, the *Phyllanthus amarus* leaf extract was found to be efficient in the biosynthesis of Ag-NP silver, as it has antimicrobial and catalytic activities [24].

Moreover, the aqueous extract of *Beta vulgaris* L. showed efficiency toward Ag-NP biosynthesis, owing to its content of vitamins, manganese, folate, and magnesium in addition to its content of pigments, with all of these factors reducing the metal ions to NPs. The pH value, extract volume, silver nitrate concentrations, and time of incubation play a vital role in Ag-NP biosynthesis [25]. The antibacterial activity of silver nanoparticles has shown potency against reference bacterial strains [17]. Recently, the diverse biological properties of *Beta vulgaris* L. and betalains have been reported [26].

Metallic/bimetallic nanoparticles have been shown to have antibacterial [27], anticancer [28], anti-inflammatory [29], and antioxidant properties [30]. The small size and large surface area of nanoparticles allow them to interact with cells and tissues [31]. The antibacterial activity of nanoparticles is attributed to their ability to disrupt the cell membranes of bacteria, leading to cell death. The nanoparticles can also generate reactive oxygen species, which can damage DNA and other cellular components [32]. Moreover, the anticancer activity of nanoparticles is related to their aptitude to kill or inhibit the growth of cancer cells or induce apoptosis or programmed cell death [33]. The anti-inflammatory activity is attributed to the aptitude of nanoparticles to inhibit the production of pro-inflammatory cytokines and other molecules and reduce inflammation by scavenging ROS and other reactive molecules [34]. Silver nanoparticles are one of the most widely studied nanoparticles for antibacterial applications. They are effective against a wide range of bacteria, including drug-resistant strains.

Herein, our study investigates the following: (i) How to biosynthesize Ag-mNPs, Ag-bmTiO₂, and Ag-bmSeO₂ using an aqueous extract of *Beta vulgaris* L. (ii) The determination of chemical features using phytochemical analyses, UV-visible spectra, FTIR, TEM, and zeta potential analyses. (iii) Assessments of the biological activities of the synthesized metallic/bimetallic nanoparticles, for instance, the antioxidant activity using DPPH and phosphomolybdate assays, and cytotoxic activity against various normal and tumor cell lines using MTT assay, as well as antimicrobial action against human bacterial pathogens.

2. Materials and Methods

2.1. Preparation of the *Beta vulgaris* Extract

Fresh root of *Beta vulgaris* was purchased from a local market in Mansoura, Egypt (latitude: 31°02'60.00" N; longitude: 31°22'59.99" E). The beets were precisely washed with tap water, and then the washing process was continued three times with distilled water. The cleaned beet was skillfully divided into small pieces and dried at room temperature until completely dry. The dried pieces (30 g) were transferred to a conical flask containing distilled water (100 mL) and soaked at 30 °C overnight. The extract obtained was filtered four times using Whatman No. 1 filter paper, centrifuged at 10,000 rpm for 10 min, and filtered again. The acquired pure extract was stored at 0–5 °C for further applications and analyses.

2.2. Biosynthesis of Silver Metallic/Bimetallic Nanoparticles

Silver, silver–selenium dioxide, and silver–titanium dioxide nanoparticle solutions were synthesized via a phytogenic green procedure [35,36]. The aqueous extract of *Beta vulgaris* L. was used to prepare these metallic and bimetallic nanoparticles. To a solution of the *Beta vulgaris* L. extract (25 mL), a solution of silver nitrate (AgNO₃) (2 mM, 25 mL) was added dropwise with continuous stirring at room temperature until the color turned brown. The reaction mixture was kept under stirring in the dark until a stable color formed. In the preparation of silver–selenium dioxide bimetallic nanoparticles (Ag–SeO₂ bmNPs), a solution of silver nitrate (2 mM) and selenium dioxide (50 mg) (Merck Schuchardt OHG, 85662, Hohenbrunn, Germany) was added dropwise to the prepared extract. Also, in the preparation of silver–titanium dioxide bimetallic nanoparticle (Ag–TiO₂

bmNPs) (Merck Schuchardt OHG, 85662, Hohenbrunn, Germany) solution, a mixture of silver nitrate (2 mM) and titanium dioxide (50 mg) solutions was added dropwise to the prepared extract under constant magnetic stirring at 25 °C. The color transformation is an indication of the formation of metallic and bimetallic nanoparticles [37]. The solutions in all cases were centrifuged for 30 min at 10,000 rpm. The precipitated solid nanoparticles were washed with distilled water and constantly washed with ethanol (85%) to remove contaminated oil. The solid materials were dried under vacuum at room temperature and stored at −80 °C for further analysis.

2.3. Instruments and Chemical Features of NPs

A UV-visible absorption spectrophotometer (Spectrophotometer UV2, Uni cam UV-VIS, Ventura, CA, USA, in the wavelength range of 190–1100 nm via a quartz cuvette of 10 mm path length) was used to investigate the optical properties of the prepared metallic/bimetallic nanoparticles. The FT-IR spectrum analysis was run at Thermo-Fisher Nicolet IS10, Waltham, MA, USA. A spectrophotometer at a resolution of 4 cm^{−1} in 500–4000 cm^{−1} was used in a transmission approach to define the contribution of the functional groups in the biosynthesis and stabilization of nanoparticles. Zeta potential analyses were run on HORIBA SZ-100 (Singapore), with a holder (24.9 °C), dispersion medium viscosity (0.897 mPa·s), conductivity (0.264 mS/cm), and electrode voltage (3.3 V). The TEM analyses were run on a ThermoFisher Talos F200i (Waltham, MA, USA) using a carbon-coated grid (Type G 200, 3.05 μ diameter, TAAP, Seattle, DC, USA) and were implemented for the characterization of size, morphology, aggregation, and crystallization of metallic/bimetallic nanoparticles. For the antioxidant activity and phytochemical analyses, a spectrophotometric apparatus (Spekol 11 spectrophotometer, analytic Jena AG, Jena, Germany) and UV lamp (Vilber Lourmat-6.LC, VILBER Smart Imaging, Marne-la-Vallée, France) were used.

2.4. Phytochemical Analysis

The phenolic contents were analyzed for the plant extract, as well as metallic/bimetallic nanoparticles using Folin–Ciocalteu (F–C) assay [38] and a gallic acid standard curve ($y = 0.0062x$, $r^2 = 0.987$). The contents of flavonoids were analyzed via aluminum chloride assay [39] using a catechin standard curve ($y = 0.0028x$, $r^2 = 0.988$). The tannin contents were analyzed via vanillin-hydrochloride assay [40] and applying the tannic acid standard curve ($y = 0.0009x$; $r^2 = 0.955$). All of the values were calculated as mg equivalents of the standard material per gram of the dried sample.

2.5. Biological Assessment

2.5.1. Antioxidant Activity

The antioxidant activity of red *Beta vulgaris* L. aqueous extract and the prepared solutions of metallic/bimetallic nanoparticles was evaluated via DPPH• assay [41]. A solution of DPPH• (0.135 mM) was used as a positive control, methanol (80%) was used as a negative control, and ascorbic acid was used as a reference standard. The samples were prepared in a serial dilution using methanol (80%). DPPH• (1 mL) was added to each tube and then incubated for 30 min at room temperature. The absorbance of each tube was recorded at 517 nm of wavelength (λ). The exponential curves were plotted for the % DPPH• remaining versus the sample concentration to estimate the values of IC₅₀ in mg/mL. The values of IC₅₀ were calculated to simplify the comparison between the results of the investigated samples, in which there was an inverse relationship between the antioxidant capacity of the sample with the IC₅₀ values [42]. The percentages of remaining DPPH• were calculated from Equation (1):

$$\text{Remaining DPPH}^\bullet (\%) = (\text{DPPH}^\bullet)_T / (\text{DPPH}^\bullet)_{T=0} \times 100 \quad (1)$$

The total antioxidant capacity was assessed via the phosphomolybdate method to investigate the antioxidant activity of *Beta vulgaris* L. extract, and metallic/bimetallic nano-solutions. A modified procedure was applied, in which the results were expressed as mg

ascorbic acid equivalent per 100 g of dry sample [43]. A freshly prepared reagent (0.6 M sulfuric acid, 28 mM sodium phosphate, 4 mM ammonium molybdate) was made. The standard reagent (3 mL) was mixed with 300 μ L of the tested sample and incubated for 90 min at 95 °C. The intensity in the blue color was measured at $\lambda = 695$ nm. A negative control was prepared by mixing the standard reagent with 300 μ L of distilled water instead of the tested sample [44].

2.5.2. Antibacterial Activity

The reference bacterial strains were provided by the Holding Company for Water and Wastewater of Egypt from the American Type Culture Collection (ATCC, Manassas, VA, USA). The tested human pathogenic bacteria were both Gram-positive (*Enterococcus faecalis* ATCC 29212/NCTC 12697 and *Staphylococcus aureus* ATCC 25923/NCTC 12981) and Gram-negative (*Escherichia coli* ATCC 8739 and *Salmonella enterica* subsp. *enterica* serovar *Typhimurium* ATCC 14028/NCTC 12023).

The preparation of standard inoculum was performed from the stock cultures by inoculating sterile glass tubes containing 10 mL nutrient broth medium (Difco, Detroit, MI, USA) with individual bacterial strains and incubating at 35 ± 1.0 °C for 24 h until turbidity was achieved equal to the 0.5 MacFarland standard (a solution mixture of barium chloride and sulfuric acid that yields a turbid fine precipitate of barium sulfate, which equals 1.5×10^8 CFU/mL). The antibacterial susceptibility test of the investigated samples was assessed using the well diffusion method [45] on Muller-Hinton agar (Difco, USA) plates. The medium was distributed in sterile Petri dishes on a level surface to a uniform depth of 4 mm in laminar flow. After solidification, a sterile cotton swab was dipped into bacterial suspension, and the surplus inoculum was eliminated by gently pressing the swab against the inner wall of the tube, positioned above the medium level; then, Muller Hinton agar plates were inoculated via streaking with the swab. The plate was allowed to stand for 5 min for the media to absorb the excess moisture. A hole of 0.5 cm diameter was made using a cork borer. Individual nanoparticles were added to each hole at 100 μ g/mL. The plates were allowed to stand for one hour in the refrigerator before being incubated (35 ± 1.0 °C for 24 h); then, they were scanned for clear zone vision, and the diameter was measured from the edge to the other edge of the clear zone area.

2.5.3. Cytotoxic Activity

Tumor and Normal Cell Lines

The cell lines of human lung fibroblast (WI38), hepatocellular carcinoma (HePG-2), and mammary gland breast cancer (MCF-7) were acquired from ATCC through a holding company for biological products and vaccines (VACSERA), Cairo, Egypt. Doxorubicin was used as a standard chemotherapeutic anticancer drug for evaluation.

MTT Assay

We carried out the MTT assay according to Denizot and Lang [46]. In this assay, the yellow color of tetrazolium bromide purchased from Sigma Co. (St. Louis, MO, USA) was transformed into a purple formazan via the action of mitochondrial succinate dehydrogenase in viable cells. Cell lines in RPMI-1640 medium (Sigma Co., St. Louis, USA) were mixed with 10% fetal bovine serum. Also, penicillin (100 units per mL) and streptomycin (100 μ g/mL) were added at 37 °C in a 5% CO₂ incubator.

The cellular cultures were placed into individual wells of a 96-well plate, with a density of 1.0×10^4 cells per well. The plate was then kept at a temperature of 37 °C for 48 h, within an environment containing 5% CO₂. Following the incubation period, the cells were exposed to various concentrations of the tested samples and then incubated for an additional 24 h. Subsequently, a solution of MTT (5 mg/mL, 20 μ L) was introduced and incubated for 4 hours. The formed purple formazan was dissolved by adding DMSO (100 μ L) (Sigma Co., St. Louis, USA) to each well. The absorbance of the color intensity of

the samples was measured as $\lambda = 570$ nm using a cuvette reader (EXL 800, Cranston, RI, USA). The percentages of relative cell viability were calculated by applying Equation (2):

$$\text{Cell viability \%} = (\text{A sample} / \text{A control "untreated sample"}) \times 100 \quad (2)$$

3. Results and Discussion

3.1. Identification of Metallic/Bimetallic Nanoparticles

Biosynthesized metallic/bimetallic nanocomposites were established using several techniques, specifically UV-visible spectra, FTIR analyses, TEM, and zeta potential analyses.

3.1.1. UV-Visible Spectra

The biosynthesized Ag, Ag-SeO₂, and Ag-TiO₂ NPs prepared using *Beta vulgaris* L. aqueous extract were characterized via UV-visible spectra (Figure 1). The *Beta vulgaris* L. extract revealed two distinctive peaks at λ_{max} ca. 554.0 nm (abs. 1.546) and λ_{max} ca. 246.0 nm (abs. 0.777); these peaks are related to the adsorption intensities of the pigment agreeing, respectively, to yellow betaxanthin and red-purple betanin [47]. The color change in the used aqueous extract in the biosynthesis of metallic/bimetallic nanoparticles was indicated through physical observation. The reddish-brown color of the prepared extract was changed into a brown color in the case of silver nanoparticles, a yellow color in the case of Ag-selenium dioxide NPs, and a gray color in the case of the preparation of Ag-titanium dioxide NPs. The nanoparticle solution of silver (Ag-mNPs) revealed surface plasmon resonance peaks at λ_{max} ca. 598.0 nm (abs. 1.632) and λ_{max} ca. 246.0 nm (abs. 0.770). The three perceived intensity peaks were recorded at λ_{max} ca. 428.0 nm (abs. 0.558), 395.0 nm (abs. 0.529), and 245.0 nm (abs. 0.791) for the biosynthesized Ag-SeO₂ bimetallic nanoparticles. Otherwise, the gray solution of Ag-TiO₂ bimetallic nanoparticles displayed two individual intensity peaks at λ_{max} ca. 675.0 nm (abs. 1.920) and 247.0 nm (abs. 0.756). The results verified the formation of metallic/bimetallic nanoparticles since the addition of the metal (Ag⁺, Ag⁺-Se²⁺, and Ag⁺-Ti²⁺) solutions into the aqueous plant extract led to an increase in the surface plasmon resonance peak at λ_{max} ca. 598.0 nm (Ag mNPs) and 675.0 nm (abs. 1.920) (Ag-TiO₂ bmNPs), and a decrease in the intensity peaks for Ag-SeO₂ bmNPs at λ_{max} ca. 428.0 nm (abs. 0.558) and 395.0 nm (abs. 0.529).

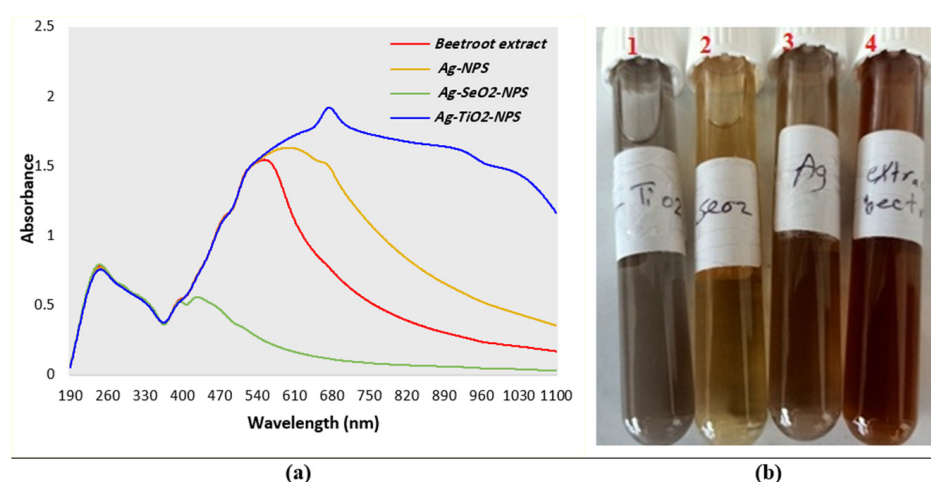


Figure 1. (a) UV-visible spectroscopy of the plant extract and nano solutions; (b) a photograph of the prepared nano-solutions: (1) Ag-TiO₂ bmNPs; (2) Ag-SeO₂ bmNPs; (3) Ag NPs; (4) *Beta vulgaris* L. aqueous extract.

3.1.2. FTIR Spectral Analyses

The FTIR spectral analyses were intended for the characterization of the major functional groups in *Beta vulgaris* L. extract such as phenolic, flavonoid components, *iso*-betanin, betanin, and vulgaxanthin, as well as the study of the role of these groups in the biosyn-

thesis of metallic/bimetallic nanoparticles. Most of the functional groups served as capping/stabilizing agents and participated in the bio-reduction process of Ag^+ ions into stable zero-valent ones (Ag^0), as well as selenium and titanium ions into the corresponding oxides. The results (Figure 2 and Table S1) indicated various frequencies owing to stretching vibrations of the distinctive functional groups, supporting the formation of metallic/bimetallic nanoparticles. Accordingly, the numerous stretching vibrations at $\nu = 3327.81$, 2105.13, 1635.99, and 421.49 cm^{-1} were perceived in the FT-IR spectrum of silver nanoparticles. The broad and strong absorption bands within wavenumbers at $\nu = 3303.81\text{--}3327.81 \text{ cm}^{-1}$ are attributed to the stretching vibrations of O-H groups, namely, phenolic hydroxyl groups. The shift in the values of these groups reinforced their involvement in proton dissociation with the aid of accomplishing the bio-reduction of the metal ions in the solution. A new absorption band in the analysis of Ag-SeO₂ bmNPs at $\nu = 3853.16 \text{ cm}^{-1}$ attributed to the O-H stretching group was also estimated for the formation of bimetallic nanoparticles. The absorption bands that appeared within the range of $\nu = 2104.77\text{--}2193.92 \text{ cm}^{-1}$ were related to the stretching vibrations of ketene, carbodiimide, or weak vibrations of alkyne. The stretching vibrations of the amidic carbonyl groups were found within $\nu = 1635.81\text{--}1636.08 \text{ cm}^{-1}$. The shift in these values of the carbonyl group revealed the role of these groups in the formation of nanoparticles. Our results agree with those previously reported [36] concerning the characterizations and interpretations of the functional groups. The absorption bands at $\nu = 1507.38$ and 1457.14 cm^{-1} are attributed to the medium bending frequencies of the C-H groups. The analysis of the plant extract revealed the presence of an absorption band at $\nu = 1045.30 \text{ cm}^{-1}$, owing to the strong stretching vibration of C-O-C or C-N of aliphatic amines. This absorption band disappeared in the FT-IT analyses of the metallic/bimetallic nanoparticle solutions, indicating the participation of these groups in the biosynthesis of these nanoparticles. Nevertheless, the absorption bands at a lower frequency, e.g., bands with wavenumbers lower than $\nu = 500 \text{ cm}^{-1}$, are attributed to the metal–metal or metal oxide bands, confirming the biosynthesis process with the patronage of the betanin of the plant extract.

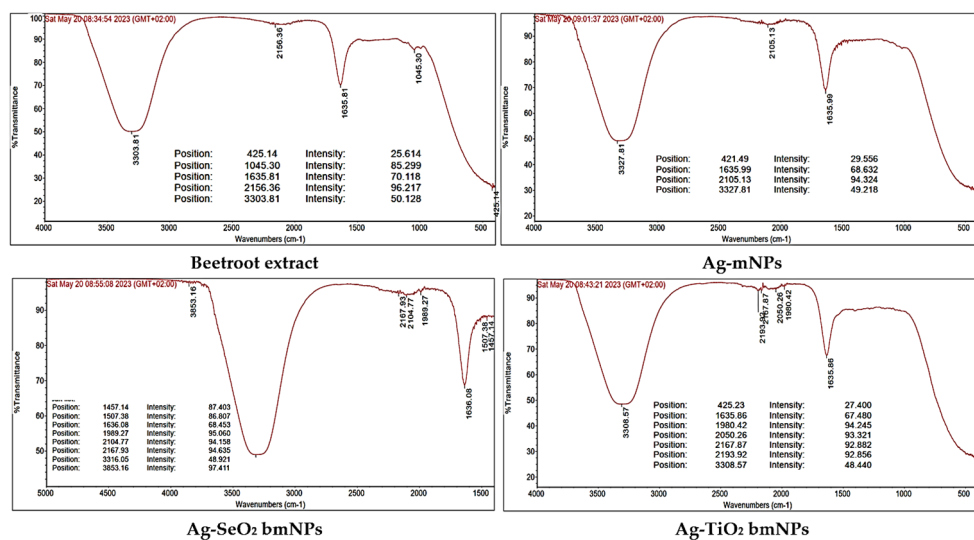


Figure 2. Charts of the FT-IR data of *Beta vulgaris* L. extract and its metallic/bimetallic nanoparticles.

3.1.3. TEM Investigation

The surface morphology, size, and aggregation attitude of the nanoparticles prepared in an eco-friendly way using an aqueous extract of *Beta vulgaris* L. were identified using TEM, as exemplified in Figure 3. The results verified that the nanoparticles have spherical shapes of a nano-scale size for all samples providing a very high surface area. The results concerning the particle size revealed varied sizes on the nanoscale, in which the Ag-mNPs demonstrated nanoparticle sizes within 12.82–21.28 nm, the Ag-SeO₂ bmNPs demonstrated

nanoparticle sizes within 8.417–18.49 nm, and the Ag-TiO₂ bmNPs demonstrated nanoparticle sizes within the size range of 12.86 to 20.09 nm. Therefore, nano-spheres were found to be agglomerated in the solution with varied sizes. The silver nanoparticles were attached to the edges of the petal surface of titanium and selenium oxides.

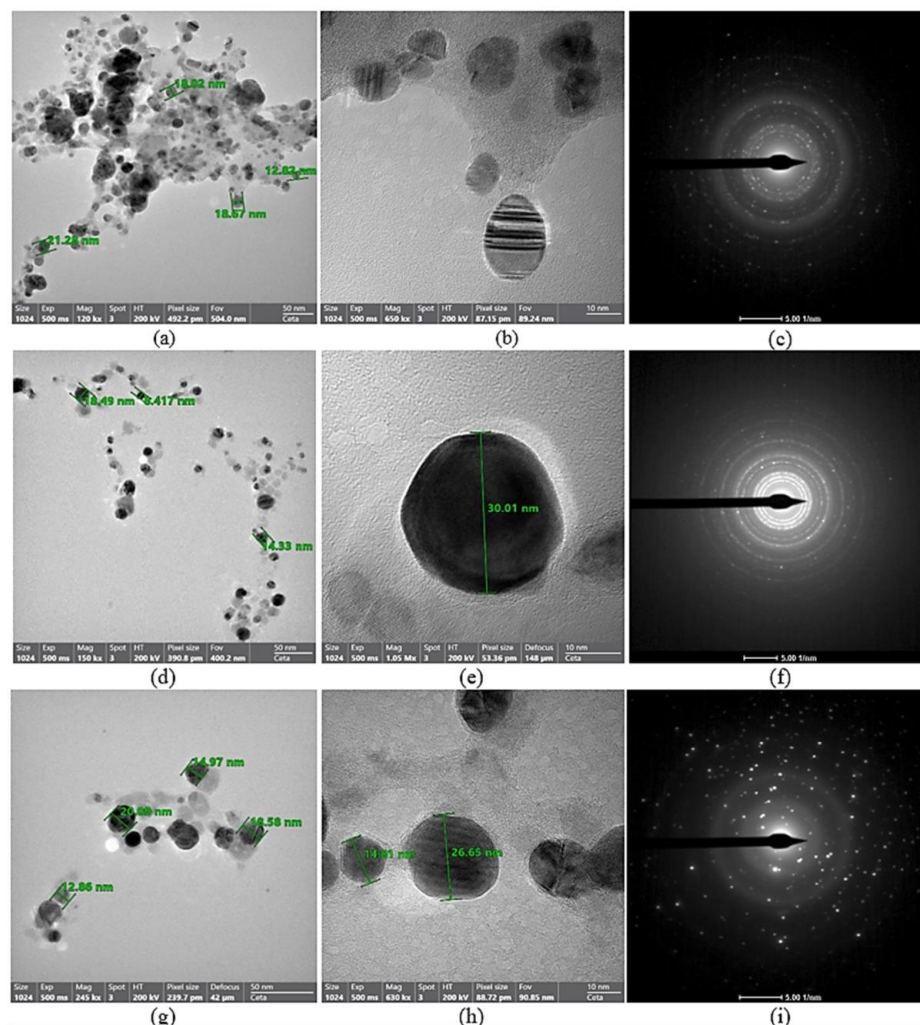


Figure 3. TEM and selected area diffraction analysis of metallic/bimetallic nanoparticles: (a,b) refer to the TEM images of the Ag-mNPs (Mag. 120 and 650 kx); (d,e) refer to the TEM images of the Ag-SeO₂ bmNPs (Mag. 150 kx and 1.05 Mx); (g,h) refer to the TEM images of the Ag-TiO₂ bmNPs (Mag. 245 and 630 kx) with Ceta = 50 and 10 nm; and (c,f,i) refer to the images of the selected area diffraction of the Ag-mNPs, Ag-SeO₂ bmNPs, and Ag-TiO₂ bmNPs, respectively.

The nucleation between silver nanoparticles and metal oxides occurred instantaneously during the preparation of bimetallic selenium and titanium nanoparticles. The interaction of metal ions in the solution with hydroxyl groups, namely phenolic groups, led to the formation of the smallest size of bimetallic oxide nanoparticles. In addition, the silver nanoparticles were formed on the surface of the metal oxides through a reduction process after the ionization of silver nitrate in the solution. The results specified the biosynthesis of metallic/bimetallic nanoparticles as they appeared from morphological analyses via the benefit of *Beta vulgaris* aqueous extract. The images of the selected area diffraction (Figure 3) revealed circulates with bright spots in the analysis of all of the samples, demonstrating the crystallinity of the formed metallic/bimetallic nanoparticles.

It was noted that the bright spots appeared more in the analysis of the Ag-TiO₂ bmNPs compared with the Ag-SeO₂ bmNPs and Ag mNPs, confirming the high level of the crystallinity of the bimetallic nanoparticles compared with the metallic silver samples

(Figure 3). Biological assessments, such as for antibacterial activity, might be controlled by the size and agglomeration state of the nanoparticles. This is a satisfactory indication that interactions between the silver nanoparticles and biomolecules might result in particle aggregation [48,49]. The agglomeration of the penetrated bimetallic silver nanoparticles revealed remarkable influences compared to Ag-mNPs, as stated by recent studies [49,50]. Consequently, owing to the higher surface area of the biosynthesized nanoparticles (spherical shapes with an average particle size lower than the nanoscale), they might employ significant antibacterial effects against the growth inhibition of various species.

3.1.4. Zeta Potential Analyses

Figure 4 displays the zeta potential analyses of the Ag-mNPs, Ag-SeO₂ bmNPs, and Ag-TiO₂ bmNPs, providing evidence concerning the charge and stability of the biosynthesized nanoparticles in the suspension. The small nanoparticles have a large surface area relative to their volume, and this surface area can be charged. The charge on the surface of the nanoparticles is counterbalanced by the presence of ions of an opposite charge in the liquid. This creates an electrical double layer around the nanoparticles. The zeta potential is the potential difference between the bulk of the liquid and the stationary layer of fluid attached to the surface of the particle. It is a measure of the strength of the electrical double layer. It was documented that zeta potential analyses are the factor controlling the estimation of the stability of the nanoparticles in the solution [51]. The results specified that Ag-mNPs revealed a mean zeta potential at -27.6 mV with a mean electrophoretic mobility of -0.000213 cm²/Vs. The Ag-SeO₂ bmNP solution displayed a mean zeta potential at -12.7 mV with a mean electrophoretic mobility = -0.000098 cm²/Vs, while the Ag-TiO₂ bmNPs revealed a mean zeta potential at -30.3 mV with a mean electrophoretic mobility = -0.000234 cm²/Vs. The results of all of the samples indicated the good stability of the biosynthesized metallic/bimetallic nanoparticles prepared from the aqueous extract of *Beta vulgaris* L.

A high value of negative charge in zeta potential analysis indicates that the particles in suspension have a strong electrostatic repulsion between them. This repulsion prevents the particles from aggregating or clumping together, which can improve the stability of the colloidal system. In general, particles with a zeta potential of ± 30 mV or more are considered to be stable. Thus, the Ag-TiO₂ bmNPs exhibited good stability with a zeta potential at -30.3 mV, followed by Ag mNPs (zeta potential = -27.6 mV), and Ag-SeO₂ bmNPs (zeta potential = -12.7 mV) had the least stability in the colloidal system.

3.2. Phytochemical Analysis

The phytochemical analyses were assessed for *Beta vulgaris* L. aqueous extract and biosynthesized metallic/bimetallic nanoparticles. In particular, the results as shown in Figure 5 and Table S2 verified that the plant extract is rich in phenolic constituents, with 65.449 ± 0.756 mg gallic acid/1 gm dry extract. The tannin contents (27.338 ± 0.24 mg tannic acid/1 gm dry extract) are higher than flavonoids (6.309 ± 0.314 mg catechine/gm dry extract) according to the analyses of the plant extract. It is worth mentioning that decreased values of phytochemicals can be seen in the analyses of metallic and bimetallic nanoparticles, verifying the contribution of these reactive species in the bio-reduction process for the biosynthesis of these nanoparticles. The comparison of the results of the metallic/bimetallic nanoparticles indicated that Ag-mNPs compromised the second order in the level of the phytochemical components. In addition, the Ag-TiO₂ bmNPs revealed higher phenolic contents than the Ag-SeO₂ bmNPs, while the Ag-SeO₂ bmNPs were marginally rich with tannin and flavonoid contents compared with the Ag-TiO₂ bmNPs. The color of *Beta vulgaris* L. is due to betanin, signifying merely 75 to 90% of the total color [52]. The investigated components of the different issues of *Beta vulgaris* L., as identified from the literature reports, were characterized as various compounds related to phenolic class, for instance, betanidin, prebetanin, isobetanin, neobetanin, amaranthin, and lampranthin [53–55].

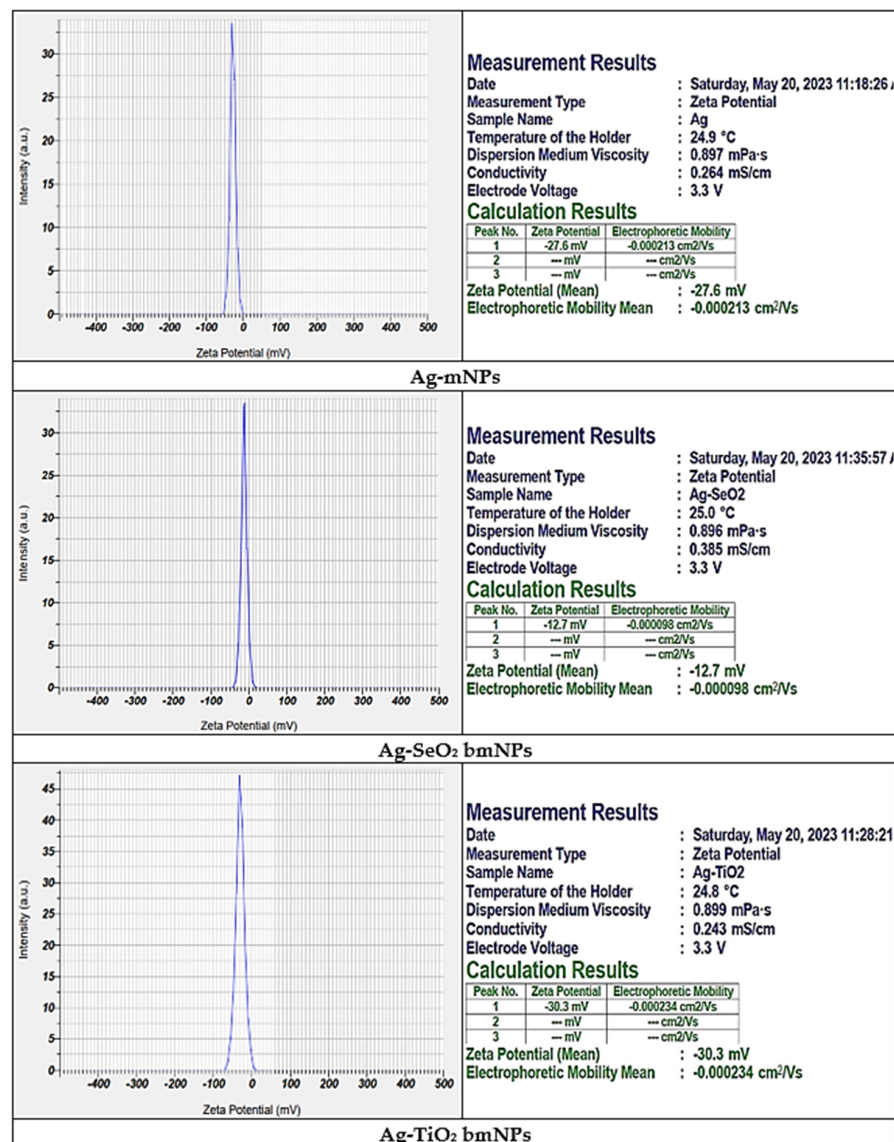


Figure 4. Zeta potential analyses of the biosynthesized metallic/bimetallic nanoparticles.

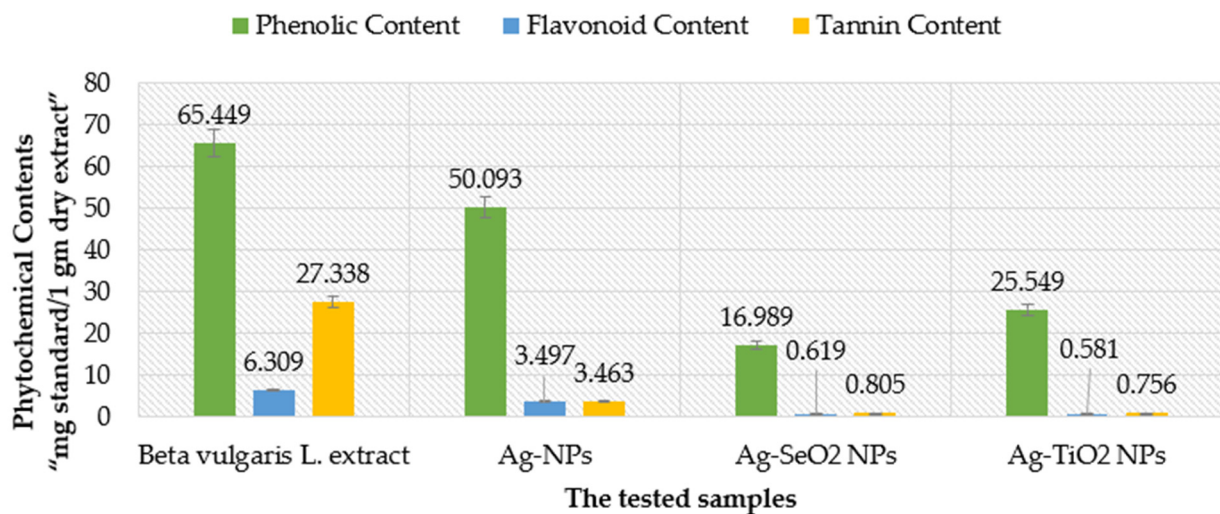


Figure 5. A comparison of the phenolic, flavonoid, and tannin contents of the tested samples.

3.3. Biological Assessments

3.3.1. Antioxidant Activity

The potential antioxidant activity was assessed for silver metallic/bimetallic nanoparticles via DPPH• free radical assay. The IC₅₀ values were calculated in mg/mL by applying the exponential curve that involved a relationship between the sample concentrations versus the percentages of the remaining DPPH• [56]. The results (Figure 6) verified that the *Beta vulgaris* L. extract revealed the most potent activity for scavenging the DPPH• free radical with IC₅₀ at 0.299 ± 0.073 mg/mL. The antioxidant capacity of the extracted *Beta vulgaris* L. was much greater using the higher concentration of the sample, and thus 74.7% inhibition was calculated at 0.902 mg/mL, while the antioxidant capacity was reduced to 32.77% at the lower concentration (0.113 mg/mL). It was noticed that the inhibition efficiencies of the tested metallic and bimetallic nanoparticle solutions were reduced compared to the aqueous extract of *Beta vulgaris* L. Accordingly, the Ag-mNPs revealed an IC₅₀ value at 0.404 ± 0.067 mg/mL, and then the antioxidant capacities were reduced again in the case of bimetallic nanoparticles, for instance, the Ag-TiO₂ bmNPs (IC₅₀ = 0.797 ± 0.063 mg/mL) and Ag-SeO₂ bmNPs (IC₅₀ = 1.473 ± 0.104 mg/mL). At the higher concentrations of the prepared nano-solutions, Ag-mNPs revealed a percentage of inhibition at 52.9% (1.958 mg/mL), the Ag-TiO₂ bmNPs revealed a percentage of inhibition at 58.08% (1.099 mg/mL), and Ag-SeO₂ bmNPs revealed a percentage of inhibition at 46.04% (1.351 mg/mL). The free radicals of DPPH• (a purple color) in the solution tended to stabilize via reactions with antioxidant molecules that are rich in stable radical sources. The stabilization of DPPH• free radicals changed the purple color of DPPH into colorless at the higher sample concentrations. The ability of the tested sample to scavenge the free radicals of DPPH• in the solution indicated the antioxidant capacity. In the case of *Beta vulgaris* extract, the hydroxyl groups provided stable hydroxyl radicals that trapped the free radicals of DPPH•. The reactive oxygen and nitrogen species in the extracted components of the plant extract are the factors that increase the antioxidant capacity. Also, the phenolic components, as estimated from the phytochemical analysis, enable the trapping of the free radicals of DPPH•. The phenolic components provided stable free radicals via the delocalization of the radical on the phenyl ring. Our results agree with the recently reported work by [57]. The release of hydrogen atoms in the antioxidant mechanism can be termed as specified in Figure 7.

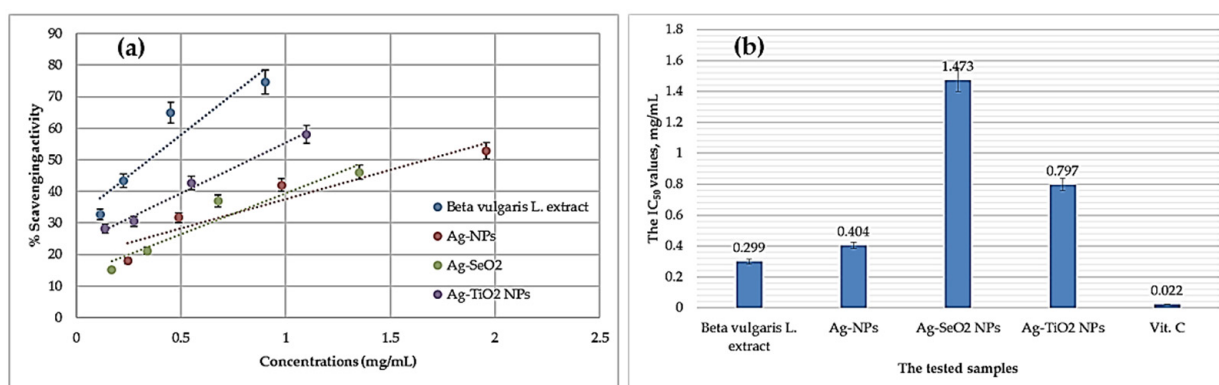


Figure 6. The antioxidant results via DPPH assay: (a) Plotted % scavenging activity versus sample concentration. (b) A comparison of the antioxidant results.

On the other hand, the antioxidant activity of aqueous *Beta vulgaris* extract and silver metallic/bimetallic nanoparticle solutions was also assessed via phosphomolybdate assay (Tables 1 and S3). The results verified that the *Beta vulgaris* extract displayed the most potent activity with total antioxidant capacity (TAC) at 2388.524 ± 7.226 (mg AAE/100 gm DS). The antioxidant activity was reduced for the Ag-mNPs (TAC = 1326.292 ± 8.835 mg AAE/100 gm DS) than the plant extract. The order of the antioxidant potency of the

samples was found that the aqueous extract was much more potent than Ag-mNPs or Ag-TiO₂ bmNPs, and Ag-SeO₂ bmNPs was the last in the order of potency. These results were matched with the antioxidant potency estimated via the DPPH free radical assay. The process relies on the reduction of phosphomolybdate ions in the presence of an antioxidant, leading to the creation of a green phosphate/Mo(V) complex. This complex is then quantitatively measured using spectrophotometry. Specifically, the antioxidants in the sample reduce the (MoO₄)²⁻ to Mo(V), in which Mo(V) forms a green phosphate/Mo(V) complex with phosphate ions (PO₄³⁻). The rich samples with antioxidants will produce the deepest color with high absorbance at $\lambda = 695$ nm as an indication of the greater antioxidant capacity. The participation of the reactive species, such as phenolic and flavonoid components of the plant extract in the reduction of metal ions through the biosynthesis of metallic/bimetallic nanoparticles, is indeed liable for their antioxidant activities [58].

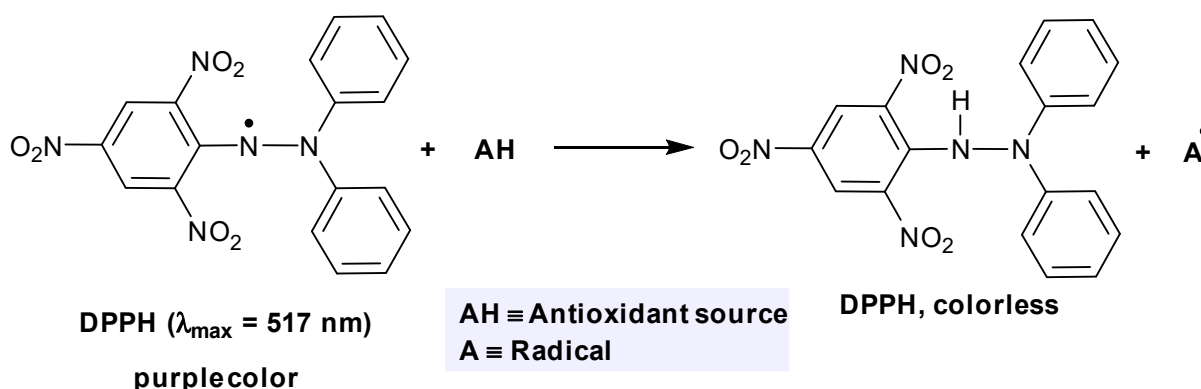


Figure 7. The planned free radical reaction between the antioxidants and DPPH[•].

Table 1. The antioxidant results using phosphomolybdate assay.

Material	Total Antioxidant Capacity (mg AAE/100 gm DS) ^(a)
Plant extract	2388.524 \pm 7.226
Ag-mNPs	1326.292 \pm 8.835
Ag-SeO ₂ bmNPs	497.994 \pm 2.364
Ag-TiO ₂ bmNPs	1142.639 \pm 5.901

^(a) mg ascorbic acid equivalent/100 gm dry sample. Values are average ($n = 3$) \pm SD.

3.3.2. Antibacterial Activity

An antibacterial bioassay of biosynthesized metallic/bimetallic oxide nanoparticles via *Beta vulgaris* extract was conducted against Gram-positive (*E. faecalis* ATTC 29212 and *S. aureus* ATTC 25923) and Gram-negative (*E. coli* ATTC 8739 and *S. enterica* ATTC 14028) human pathogens. The agar diffusion method was applied at 100 μ g/mL. Generally, all tested nanoparticles showed antibacterial activity to various degrees. However, the Ag-SeO₂ bmNPs had superiority compared to the other ones, followed by the Ag-TiO₂ NPs (Table 2 and Figure S1). The Gram-positive bacteria were more sensitive to the tested nanoparticles than the Gram-negative ones. Among bacteria, *S. aureus* is greatly affected by nanoparticles, especially the Ag-SeO₂ bmNPs followed by *E. faecalis* and *S. enterica*. On the other hand, *E. coli* was shown to be less susceptible to the tested nanoparticles, except for the Ag-NPs, which showed more potentiality than the other ones.

Table 2. Antibacterial activity of mono- and bimetallic silver-based nanoparticles against some human pathogenic bacteria (average \pm SD, $n = 3$). The aqueous *Beta vulgaris* L. extract showed no antibacterial activity.

Bacterium	Nanoparticle	Hallow Zone Diameter (mm)
<i>S. aureus</i>	Ag-NPs	16.7 \pm 1.1
	Ag-SeO ₂ -NPs	37.7 \pm 2.1
	Ag-TiO ₂ -NPs	21.3 \pm 0.6
<i>E. faecalis</i>	Ag-NPs	14.0 \pm 1.3
	Ag-SeO ₂ -NPs	34.7 \pm 1.6
	Ag-TiO ₂ -NPs	20.0 \pm 2.6
<i>E. coli</i>	Ag-NPs	16.7 \pm 0.8
	Ag-SeO ₂ -NPs	11.7 \pm 0.6
	Ag-TiO ₂ -NPs	11.0 \pm 1.0
<i>S. enterica</i>	Ag-NPs	19.7 \pm 2.1
	Ag-SeO ₂ -NPs	32.7 \pm 1.2
	Ag-TiO ₂ -NPs	25.0 \pm 1.0

The activity of silver nanoparticles was observed against *Streptococcus mutans*, *Escherichia coli*, and *Staphylococcus aureus* [59]. The kinetic process of silver nanoparticles against bacterial species could be hypothesized for different mechanisms: (i) Penetration into bacterial cell membranes, changing the structure of the cell membrane, and even resulting in cell death. (ii) The efficacy of nanoparticle activity could not depend upon the nanoscale but was also due to their large ratio of surface area to volume. (iii) Another hypothesis is that, during the penetration of nanoparticles into the cell membrane, the reactive oxygen species are generated and interrupt the replication of deoxyribonucleic acid via the released silver ions [60]. (iv) Additionally, the titanium nanotube surfaces containing silver, copper, zinc, or selenium showed antibacterial activity toward *Staphylococcus epidermis* DSM3269 [61]. Our results matched with the previous study of Filipović, et al. [62] that found that selenium nanoparticles were found to have antimicrobial activity against *Staphylococcus aureus* (ATCC6538), *E. coli* (ATCC8739), *Enterococcus faecalis* (ATCC29212), *Bacillus subtilis* (ATCC6633), *Salmonella* sp., *Klebsiella pneumoniae* (NCIMB9111), and *Pseudomonas aeruginosa* (ATCC9027).

The successful synthesis of these eco-friendly nanoparticles with potent antibacterial properties opens up new avenues for medical applications. These nanoparticles have the potential to revolutionize alternate therapies and contribute to the development of environmentally sustainable nanomedicines for combating bacterial infections. Additionally, the study paves the way for future research into utilizing nature-inspired approaches for green and effective medical advancements.

3.3.3. Cytotoxic Activity

The cytotoxic activity of the biosynthesized Ag-NPs, the Ag-TiO₂ bmNPs, Ag-SeO₂ bmNP nanoparticles, and *Beta vulgaris* aqueous extract was evaluated in vitro, applying the MTT assay (Figure 8 and Table S4). WI38 was used as a normal cell line, and HePG2 and MCF-7 were applied as tumor cell lines. The results specified that *Beta vulgaris* extract revealed the least cytotoxic potency against the tumor cell lines, specifically HePG2 with IC₅₀ = 67.96 \pm 3.7 μ g/mL and MCF-7 cell lines with IC₅₀ = 59.20 \pm 3.3 μ g/mL. It was significant that the formation of metallic/bimetallic nanoparticles improved the cytotoxicity against the inhibition of cell line growth. Particularly, the Ag NPs revealed improved cytotoxicity against the HePG2 (IC₅₀ = 39.69 \pm 2.3 μ g/mL) and MCF-7 (IC₅₀ = 45.40 \pm 2.5 μ g/mL) cell lines in comparison with the results of the plant

extract. Furthermore, the formation of bimetallic nanoparticles improved the cytotoxicity against the tumor cell lines in comparison to the cytotoxic effects of silver nanoparticles. Thus, the Ag-TiO₂ bmNPs revealed strong cytotoxicity against the HePG2 cell line (IC₅₀ = 18.18 ± 1.5 µg/mL). In addition, the Ag-SeO₂ bmNPs displayed a strong cytotoxic effect against the MCF-7 cell line (IC₅₀ = 17.92 ± 1.4 µg/mL). In comparison with the results with doxorubicin, it was noted that the Ag-TiO₂ bmNPs and Ag-SeO₂ bmNPs were the most effective cytotoxic agents acquired from a bio-source, with fewer side effects on the growth of the normal cell line (WI38). Ag-TiO₂ bmNPs are the most appropriate cytotoxic agent against the WI38 cell line, with IC₅₀ = 83.39 ± 4.1 µg/mL; this led to the highest percentage of cell viability.

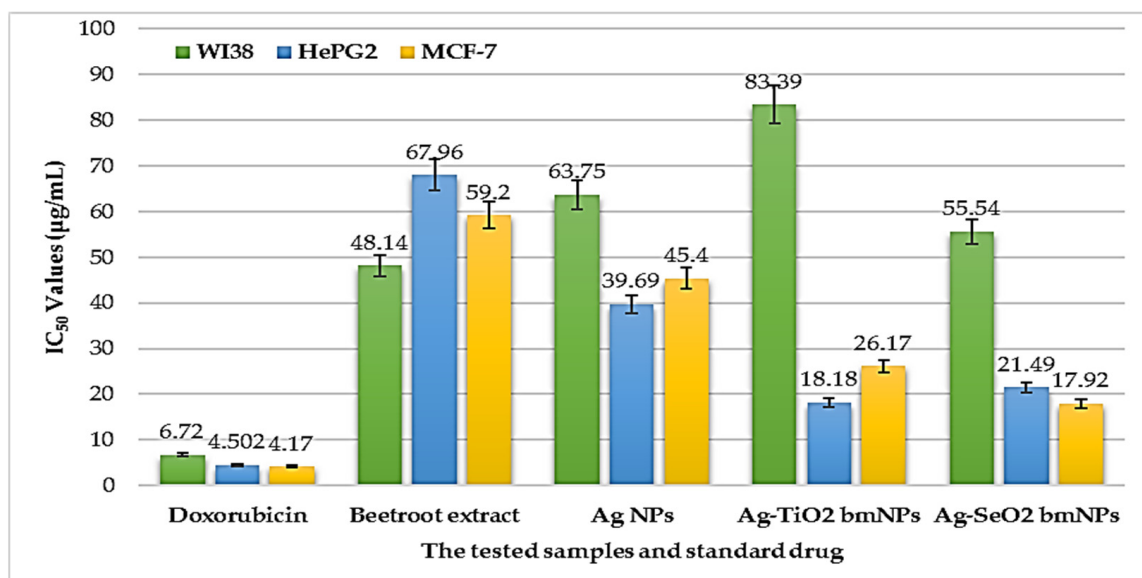


Figure 8. Comparison of the cytotoxic results against the various tumor and normal cell lines.

Figures 9 and S2 and Table S5 introduce the percentages of cell viability at different concentrations (1.56–100 µg/mL). The high dose of the samples led to the improved % inhibition against the cell growth in line with the least cell viability. At 100 µg/mL, the Ag-SeO₂ bmNPs displayed the most reduced % of cell viability against both types of tumor cell lines. It still remains that doxorubicin has a great impact on the growth of tumors and normal cell lines. The Ag-TiO₂ bmNPs displayed the most improved cytotoxicity against WI38 cells, with 48.2% viability; at the same time, this nano-solution has good cytotoxicity against the following tumor cell lines: HePG2: 21.4% and MCF-7: 28.3%. The decrease in the dose concentration resulted in increased cell viability percentages. Silver nanoparticles have the most potent cytotoxic effect against WI38 cells at 12.5 µg/mL (93.5%) and have no cytotoxic action at 6.25 and 3.125 µg/mL.

The mechanism of the cytotoxicity of metal nanoparticles against WI38, HePG2, and MCF7 is not fully understood, but it is thought to involve a combination of factors, including surface morphology of the nanoparticles, size, shape, surface defects, and bioaccumulation [63]. Precisely, the surface chemistry [64] of metal nanoparticles can affect their toxicity, in which positively charged nanoparticles are more likely to interact with cell membranes and cause damage. Smaller [65] and needle-shaped [66] nanoparticles are more likely to enter cells and cause damage. The presence of surface defects [67] on metal nanoparticles can also affect their toxicity. These defects can act as sites for the generation of reactive oxygen species (ROS), which can damage cells. The relative importance of these mechanisms may vary depending on the metal nanoparticle, the cell type, and the exposure conditions. For example, some metal nanoparticles may be more cytotoxic to WI38 cells than HePG2 cells [68]. In addition to these mechanisms, metal nanoparticles may also have other effects that contribute to their cytotoxicity. For example, metal nanoparticles

can induce inflammation, which can damage cells. Silver nanoparticles can generate ROS, which can damage DNA and other cellular components [69]. Silver nanoparticles can also induce apoptosis by activating caspases [33]. It is important to note that the cytotoxicity of metal nanoparticles can vary depending on the specific nanoparticle and the exposure conditions [70]. Additionally, the toxicity of metal nanoparticles can be increased by the presence of other chemicals, such as organic solvents or surfactants.

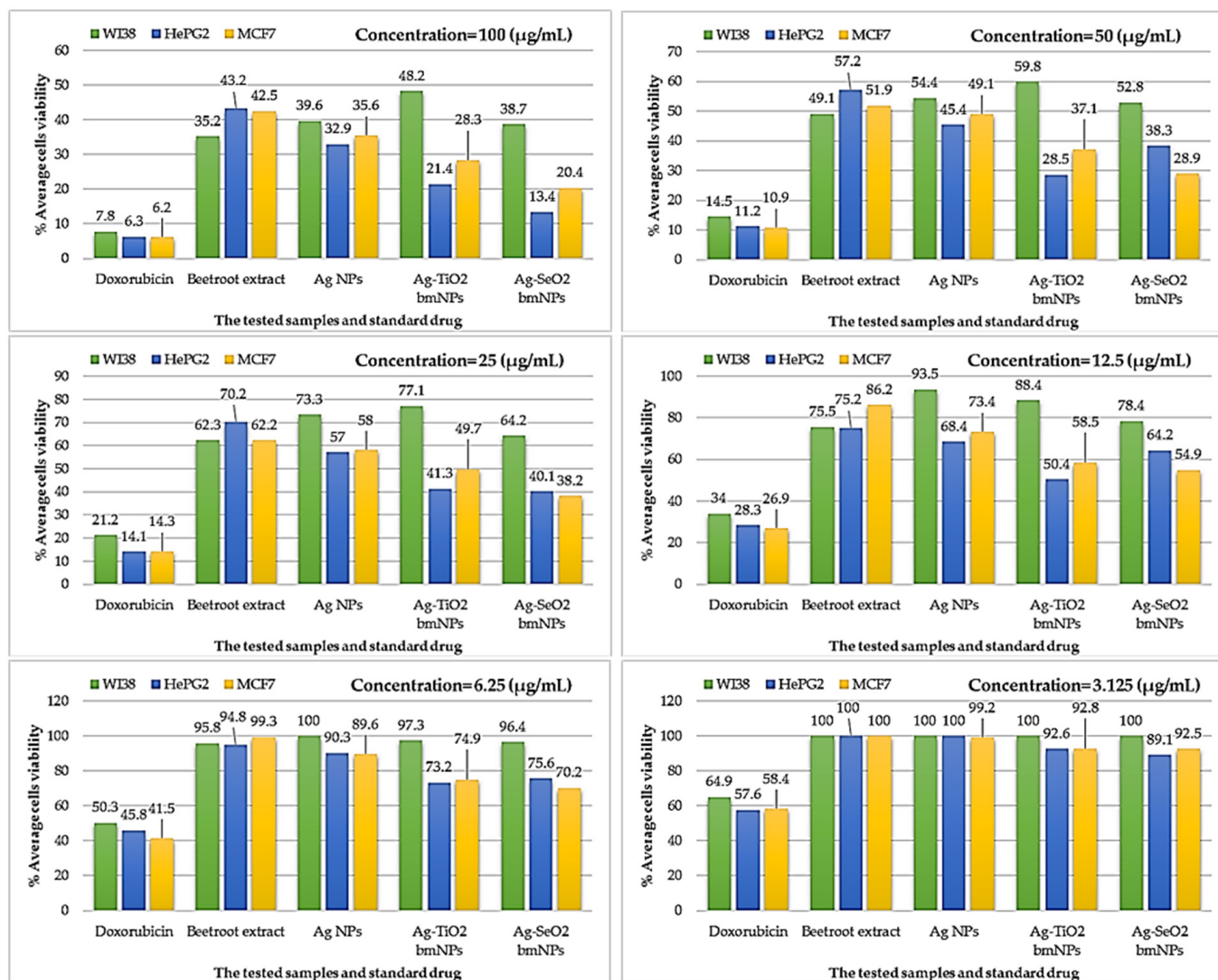


Figure 9. Comparison of the percentages of cell viability at different concentrations.

4. Conclusions

Beta vulgaris L. extract was used as a reducing and capping agent, as it is eco-friendly and can be easily scaled up for the phytochemical synthesis of metallic silver/bimetallic nanoparticles. These nanoparticles were characterized using a variety of techniques, including UV-Vis spectroscopy, FTIR, TEM, and zeta potential analyses, to investigate their optical properties, functional groups, surface morphology, size, shape, and aggregation of nanoparticles. The antioxidant, antibacterial, and cytotoxic activities of *Beta vulgaris* extract as well as nanoparticles were assessed using a variety of in vitro assays. The metallic/bimetallic nanoparticles revealed reduced phytochemical constituents compared with the plant extract, thus reducing their antioxidant capacity. This performance is attributed to the participation of the phenolic hydroxyl groups in the bio-reduction of metal ions in the solution. The metallic/bimetallic nanoparticles displayed improved antibacterial

activity against the variety of bacterial species; this is attributed to the large surface area and aggregation factors of the nanoparticles. In addition, the in vitro cytotoxic assessment of metallic/bimetallic nanoparticles revealed strong cytotoxicity against the HePG2 and MCF7 cell lines, with decreased cell viability percentages, by increasing the sample dose. The phytochemical analyses indicated the significance of phenolic, flavonoid, and tannin contents for developing biological activities with targeted therapeutic effects. In conclusion, the biosynthesis of nanoparticles, characterization of nanoparticles, biological assessments, and phytochemical analyses are all critical aspects of the development of safe and effective nanoparticles for biomedical applications.

Supplementary Materials: The following supporting information can be downloaded at <https://www.mdpi.com/article/10.3390/app131810110/s1>: Tables S1–S5 and Figures S1 and S2.

Author Contributions: Conceptualization, K.M.E., M.S.E.-H. and W.I.A.S.; data curation, K.M.E. and A.A.G.; formal analysis, K.M.E., A.A.G., F.O.A.-O. and Y.A.H.; funding acquisition, F.O.A.-O.; investigation, K.M.E. and A.A.G.; methodology, K.M.E., A.A.G. and F.O.A.-O.; resources, F.O.A.-O. and Y.A.H.; software, F.O.A.-O. and Y.A.H.; supervision, W.I.A.S.; validation, K.M.E., M.S.E.-H., Y.A.H. and W.I.A.S.; visualization, M.S.E.-H.; writing—original draft, M.S.E.-H.; writing—review and editing, K.M.E. and W.I.A.S. All authors have read and agreed to the published version of the manuscript.

Funding: The authors extend their appreciation to the Researchers Supporting Project, number RSP2023R114, King Saud University, Riyadh, Saudi Arabia.

Institutional Review Board Statement: Not applicable.

Informed Consent Statement: Not applicable.

Data Availability Statement: All data generated or analyzed during this study are included in this published article and the Supplementary File Materials.

Conflicts of Interest: The authors declare no conflict of interest.

References

1. Sharma, V.K.; Sayes, C.M.; Guo, B.; Pillai, S.; Parsons, J.G.; Wang, C.; Yan, B.; Ma, X. Interactions between silver nanoparticles and other metal nanoparticles under environmentally relevant conditions: A review. *Sci. Total Environ.* **2019**, *653*, 1042–1051. [[CrossRef](#)]
2. Bäuerlein, P.S.; Emke, E.; Tromp, P.; Hofman, J.A.; Carboni, A.; Schooneman, F.; de Voogt, P.; van Wezel, A.P. Is there evidence for man-made nanoparticles in the Dutch environment? *Sci. Total Environ.* **2017**, *576*, 273–283. [[CrossRef](#)] [[PubMed](#)]
3. Ahn, E.C.; Wong, H.-S.P.; Pop, E. Carbon nanomaterials for non-volatile memories. *Nat. Rev. Mater.* **2018**, *3*, 18009. [[CrossRef](#)]
4. Yu, X.; Cheng, H.; Zhang, M.; Zhao, Y.; Qu, L.; Shi, G. Graphene-based smart materials. *Nat. Rev. Mater.* **2017**, *2*, 17046. [[CrossRef](#)]
5. Tong, T.; Wilke, C.M.; Wu, J.; Binh, C.T.T.; Kelly, J.J.; Gaillard, J.-F.; Gray, K.A. Combined toxicity of nano-ZnO and nano-TiO₂: From single-to multinanomaterial systems. *Environ. Sci. Technol.* **2015**, *49*, 8113–8123. [[CrossRef](#)]
6. Wimmer, A.; Kalinnik, A.; Schuster, M. New insights into the formation of silver-based nanoparticles under natural and semi-natural conditions. *Water Res.* **2018**, *141*, 227–234. [[CrossRef](#)]
7. Manfra, L.; Rotini, A.; Bergami, E.; Grassi, G.; Faleri, C.; Corsi, I. Comparative ecotoxicity of polystyrene nanoparticles in natural seawater and reconstituted seawater using the rotifer *Brachionus plicatilis*. *Ecotoxicol. Environ. Saf.* **2017**, *145*, 557–563. [[CrossRef](#)]
8. Yang, Y.; Chen, B.; Hower, J.; Schindler, M.; Winkler, C.; Brandt, J.; Di Giulio, R.; Ge, J.; Liu, M.; Fu, Y. Discovery and ramifications of incidental Magnéli phase generation and release from industrial coal-burning. *Nat. Commun.* **2017**, *8*, 194. [[CrossRef](#)]
9. Goodwin Jr, D.G.; Adeleye, A.S.; Sung, L.; Ho, K.T.; Burgess, R.M.; Petersen, E.J. Detection and quantification of graphene-family nanomaterials in the environment. *Environ. Sci. Technol.* **2018**, *52*, 4491–4513. [[CrossRef](#)]
10. Schindler, M.; Hochella, M.F. Sequestration of Pb–Zn–Sb- and As-bearing incidental nanoparticles by mineral surface coatings and mineralized organic matter in soils. *Environ. Sci. Process. Impacts* **2017**, *19*, 1016–1027. [[CrossRef](#)]
11. Hochella, M.F.; Spencer, M.G.; Jones, K.L. Nanotechnology: Nature’s gift or scientists’ brainchild? *Environ. Sci. Nano* **2015**, *2*, 114–119. [[CrossRef](#)]
12. Wilke, C.M.; Wunderlich, B.; Gaillard, J.-F.; Gray, K.A. Synergistic bacterial stress results from exposure to nano-Ag and nano-TiO₂ mixtures under light in environmental media. *Environ. Sci. Technol.* **2018**, *52*, 3185–3194. [[CrossRef](#)]
13. Kesharwani, P.; Gorain, B.; Low, S.Y.; Tan, S.A.; Ling, E.C.S.; Lim, Y.K.; Chin, C.M.; Lee, P.Y.; Lee, C.M.; Ooi, C.H. Nanotechnology based approaches for anti-diabetic drugs delivery. *Diabetes Res. Clin. Pract.* **2018**, *136*, 52–77. [[CrossRef](#)]
14. Saravanan, M.; Barik, S.K.; MubarakAli, D.; Prakash, P.; Pugazhendhi, A. Synthesis of silver nanoparticles from *Bacillus brevis* (NCIM 2533) and their antibacterial activity against pathogenic bacteria. *Microb. Pathog.* **2018**, *116*, 221–226. [[CrossRef](#)] [[PubMed](#)]

15. Oves, M.; Aslam, M.; Rauf, M.A.; Qayyum, S.; Qari, H.A.; Khan, M.S.; Alam, M.Z.; Tabrez, S.; Pugazhendhi, A.; Ismail, I.M. Antimicrobial and anticancer activities of silver nanoparticles synthesized from the root hair extract of *Phoenix dactylifera*. *Mater. Sci. Eng. C* **2018**, *89*, 429–443. [[CrossRef](#)] [[PubMed](#)]
16. Samuel, M.S.; Jose, S.; Selvarajan, E.; Mathimani, T.; Pugazhendhi, A. Biosynthesized silver nanoparticles using *Bacillus amyloliquefaciens*; Application for cytotoxicity effect on A549 cell line and photocatalytic degradation of p-nitrophenol. *J. Photochem. Photobiol. B Biol.* **2020**, *202*, 111642. [[CrossRef](#)]
17. Mehdizadeh, S.; Ghasemi, N.; Ramezani, M. The synthesis of silver nanoparticles using Beetroot extract and its antibacterial and catalytic activity. *Eurasian Chem. Commun.* **2019**, *1*, 545–558.
18. Tajik, S.; Beitollahi, H.; Dourandish, Z.; Mohammadzadeh Jahani, P.; Sheikhshoae, I.; Askari, M.B.; Salarizadeh, P.; Nejad, F.G.; Kim, D.; Kim, S.Y. Applications of non-precious transition metal oxide nanoparticles in electrochemistry. *Electroanalysis* **2022**, *34*, 1065–1091. [[CrossRef](#)]
19. Babu, M.G.; Gunasekaran, P. Production and structural characterization of crystalline silver nanoparticles from *Bacillus cereus* isolate. *Colloids Surf. B Biointerfaces* **2009**, *74*, 191–195. [[CrossRef](#)]
20. Powar, N.; Patel, V.; Pagare, P.; Pandav, R. Cu nanoparticle: Synthesis, characterization and application. *Chem. Methodol* **2019**, *3*, 457–480.
21. Song, J.Y.; Kim, B.S. Rapid biological synthesis of silver nanoparticles using plant leaf extracts. *Bioprocess Biosyst. Eng.* **2009**, *32*, 79–84. [[CrossRef](#)] [[PubMed](#)]
22. Gardea-Torresdey, J.L.; Gomez, E.; Peralta-Videa, J.R.; Parsons, J.G.; Troiani, H.; Jose-Yacaman, M. Alfalfa sprouts: A natural source for the synthesis of silver nanoparticles. *Langmuir* **2003**, *19*, 1357–1361. [[CrossRef](#)]
23. Ahmad, N.; Sharma, S. Green synthesis of silver nanoparticles using extracts of *Ananas comosus*. *Green Sustain. Chem.* **2012**, *2*, 141–147. [[CrossRef](#)]
24. Ajitha, B.; Reddy, Y.A.K.; Jeon, H.-J.; Ahn, C.W. Synthesis of silver nanoparticles in an eco-friendly way using *Phyllanthus amarus* leaf extract: Antimicrobial and catalytic activity. *Adv. Powder Technol.* **2018**, *29*, 86–93. [[CrossRef](#)]
25. Thiruvengadam, M.; Chung, I.-M.; Samynathan, R.; Chandar, S.H.; Venkidasamy, B.; Sarkar, T.; Rebezov, M.; Gorelik, O.; Shariati, M.A.; Simal-Gandara, J. A comprehensive review of beetroot (*Beta vulgaris* L.) bioactive components in the food and pharmaceutical industries. *Crit. Rev. Food Sci. Nutr.* **2022**, 1–33. [[CrossRef](#)]
26. Hadipour, E.; Taleghani, A.; Tayarani-Najaran, N.; Tayarani-Najaran, Z. Biological effects of red beetroot and betalains: A review. *Phytother. Res.* **2020**, *34*, 1847–1867. [[CrossRef](#)]
27. Singh, C.; Mehata, A.K.; Priya, V.; Malik, A.K.; Setia, A.; Suseela, M.N.L.; Vikas; Gokul, P.; Samridhi; Singh, S.K. Bimetallic Au–Ag nanoparticles: Advanced nanotechnology for tackling antimicrobial resistance. *Molecules* **2022**, *27*, 7059. [[CrossRef](#)]
28. Elemike, E.E.; Onwudiwe, D.C.; Nundkumar, N.; Singh, M.; Iyekowa, O. Green synthesis of Ag, Au and Ag–Au bimetallic nanoparticles using *Stigmaphyllon ovatum* leaf extract and their in vitro anticancer potential. *Mater. Lett.* **2019**, *243*, 148–152. [[CrossRef](#)]
29. Saeed, A.; Akhtar, M.; Zulfikar, S.; Hanif, F.; Alsafari, I.A.; Agboola, P.O.; Haider, S.; Warsi, M.F.; Shakir, I. Thiamine-functionalized silver–copper bimetallic nanoparticles-based electrochemical sensor for sensitive detection of anti-inflammatory drug 4-aminoantipyrine. *Chem. Pap.* **2022**, *76*, 2721–2731. [[CrossRef](#)]
30. Imraish, A.; Abu Thiab, T.; Al-Awaida, W.; Al-Ameer, H.J.; Bustanji, Y.; Hammad, H.; Alsharif, M.; Al-Hunaiti, A. In vitro anti-inflammatory and antioxidant activities of ZnFe₂O₄ and CrFe₂O₄ nanoparticles synthesized using *Boswellia carteri* resin. *J. Food Biochem.* **2021**, *45*, e13730. [[CrossRef](#)]
31. Hewitt, R.E.; Chappell, H.F.; Powell, J.J. Small and dangerous? Potential toxicity mechanisms of common exposure particles and nanoparticles. *Curr. Opin. Toxicol.* **2020**, *19*, 93–98. [[CrossRef](#)]
32. Angelé-Martínez, C.; Nguyen, K.V.T.; Ameer, F.S.; Anker, J.N.; Brumaghim, J.L. Reactive oxygen species generation by copper (II) oxide nanoparticles determined by DNA damage assays and EPR spectroscopy. *Nanotoxicology* **2017**, *11*, 278–288. [[CrossRef](#)] [[PubMed](#)]
33. Ullah, I.; Khalil, A.T.; Ali, M.; Iqbal, J.; Ali, W.; Alarifi, S.; Shinwari, Z.K. Green-synthesized silver nanoparticles induced apoptotic cell death in MCF-7 breast cancer cells by generating reactive oxygen species and activating caspase 3 and 9 enzyme activities. *Oxidative Med. Cell. Longev.* **2020**, *2020*, 1215395. [[CrossRef](#)] [[PubMed](#)]
34. Abdelhafez, O.H.; Ali, T.F.S.; Fahim, J.R.; Desoukey, S.Y.; Ahmed, S.; Behery, F.A.; Kamel, M.S.; Gulder, T.A.; Abdelmohsen, U.R. Anti-inflammatory potential of green synthesized silver nanoparticles of the soft coral *Nephthea* sp. supported by metabolomics analysis and docking studies. *Int. J. Nanomed.* **2020**, *15*, 5345–5360. [[CrossRef](#)]
35. Helmy, E.T.; Ayyad, M.A.; Ali, M.A.; Mohamedbaker, H.; Pan, J.H. Biochemical, Histological Changes, Protein Electrophoretic Pattern, and Field Application of CuPb–Ferrite/TiO₂ Nanocomposites for Controlling Terrestrial Gastropod *Eobania vermiculata* (Müller). *J. Agric. Food Chem.* **2023**, *71*, 6626–6634. [[CrossRef](#)] [[PubMed](#)]
36. Kamli, M.R.; Srivastava, V.; Hajrah, N.H.; Sabir, J.S.; Ali, A.; Malik, M.A.; Ahmad, A. Phytogenic fabrication of Ag–Fe Bimetallic nanoparticles for cell cycle arrest and apoptosis signaling pathways in *Candida auris* by generating oxidative stress. *Antioxidants* **2021**, *10*, 182. [[CrossRef](#)]
37. Soni, M.; Mehta, P.; Soni, A.; Goswami, G.K. Green nanoparticles: Synthesis and applications. *IOSR J. Biotechnol. Biochem.* **2018**, *4*, 78–83.
38. Sánchez-Rangel, J.C.; Benavides, J.; Heredia, J.B.; Cisneros-Zevallos, L.; Jacobo-Velázquez, D.A. The Folin–Ciocalteu assay revisited: Improvement of its specificity for total phenolic content determination. *Anal. Methods* **2013**, *5*, 5990–5999. [[CrossRef](#)]

39. Zhishen, J.; Mengcheng, T.; Jianming, W. Research on antioxidant activity of flavonoids from natural materials. *Food Chem* **1999**, *64*, e9.
40. Aberoumand, A. Nutritional evaluation of edible *Portulaca oleracia* as plant food. *Food Anal. Methods* **2009**, *2*, 204–207. [[CrossRef](#)]
41. Kitts, D.D.; Wijewickreme, A.N.; Hu, C. Antioxidant properties of a North American ginseng extract. *Mol. Cell. Biochem.* **2000**, *203*, 1–10. [[CrossRef](#)] [[PubMed](#)]
42. Parejo, I.; Codina, C.; Petrakis, C.; Kefalas, P. Evaluation of scavenging activity assessed by Co (II)/EDTA-induced luminol chemiluminescence and DPPH-(2,2-diphenyl-1-picrylhydrazyl) free radical assay. *J. Pharmacol. Toxicol. Methods* **2000**, *44*, 507–512. [[CrossRef](#)] [[PubMed](#)]
43. Prieto, P.; Pineda, M.; Aguilar, M. Spectrophotometric quantitation of antioxidant capacity through the formation of a phosphomolybdenum complex: Specific application to the determination of vitamin E. *Anal. Biochem.* **1999**, *269*, 337–341. [[CrossRef](#)]
44. Belyagoubi-Benhammou, N.; Belyagoubi, L.; Gismondi, A.; Di Marco, G.; Canini, A.; Atik Bekkara, F. GC/MS analysis, and antioxidant and antimicrobial activities of alkaloids extracted by polar and apolar solvents from the stems of *Anabasis articulata*. *Med. Chem. Res.* **2019**, *28*, 754–767. [[CrossRef](#)]
45. Zerrad, A.; Anissi, J.; Ghanam, J.; Sendide, K.; El Hassouni, M. Antioxidant and antimicrobial activities of melanin produced by a *Pseudomonas balearica* strain. *J. Biotechnol. Lett.* **2014**, *5*, 87–94.
46. Denizot, F.; Lang, R. Rapid colorimetric assay for cell growth and survival: Modifications to the tetrazolium dye procedure giving improved sensitivity and reliability. *J. Immunol. Methods* **1986**, *89*, 271–277. [[CrossRef](#)] [[PubMed](#)]
47. Crane, R.A.; Scott, T.B. Nanoscale zero-valent iron: Future prospects for an emerging water treatment technology. *J. Hazard. Mater.* **2012**, *211*, 112–125. [[CrossRef](#)]
48. Argentièrè, S.; Cella, C.; Cesaria, M.; Milani, P.; Lenardi, C. Silver nanoparticles in complex biological media: Assessment of colloidal stability and protein corona formation. *J. Nanopart. Res.* **2016**, *18*, 253. [[CrossRef](#)]
49. Lankoff, A.; Sandberg, W.J.; Wegierek-Ciuk, A.; Lisowska, H.; Refsnes, M.; Sartowska, B.; Schwarze, P.E.; Meczynska-Wielgosz, S.; Wojewodzka, M.; Kruszewski, M. The effect of agglomeration state of silver and titanium dioxide nanoparticles on cellular response of HepG2, A549 and THP-1 cells. *Toxicol. Lett.* **2012**, *208*, 197–213. [[CrossRef](#)]
50. Bae, E.; Lee, B.-C.; Kim, Y.; Choi, K.; Yi, J. Effect of agglomeration of silver nanoparticle on nanotoxicity depression. *Korean J. Chem. Eng.* **2013**, *30*, 364–368. [[CrossRef](#)]
51. Hebbalalu, D.; Lalley, J.; Nadagouda, M.N.; Varma, R.S. Greener techniques for the synthesis of silver nanoparticles using plant extracts, enzymes, bacteria, biodegradable polymers, and microwaves. *ACS Sustain. Chem. Eng.* **2013**, *1*, 703–712. [[CrossRef](#)]
52. Hendry, G.A.F.; Houghton, J. *Natural Food Colorants*; Springer Science & Business Media: Berlin/Heidelberg, Germany, 1996; pp. 40–79.
53. Bokern, M.; Heuer, S.; Wray, V.; Witte, L.; Macek, T.; Vanek, T.; Strack, D. Ferulic acid conjugates and betacyanins from cell cultures of *Beta vulgaris*. *Phytochemistry* **1991**, *30*, 3261–3265. [[CrossRef](#)]
54. Jackman, R.; Smith, J. Anthocyanins and betalains. In *Natural Food Colorants*; Springer: Berlin/Heidelberg, Germany, 1996; pp. 244–309.
55. Kujala, T.S.; Loponen, J.M.; Klika, K.D.; Pihlaja, K. Phenolics and betacyanins in red beetroot (*Beta vulgaris*) root: Distribution and effect of cold storage on the content of total phenolics and three individual compounds. *J. Agric. Food Chem.* **2000**, *48*, 5338–5342. [[CrossRef](#)]
56. Brand-Williams, W.; Cuvelier, M.-E.; Berset, C. Use of a free radical method to evaluate antioxidant activity. *LWT Food Sci. Technol.* **1995**, *28*, 25–30. [[CrossRef](#)]
57. Al-Asfar, A.; Zaheer, Z.; Aazam, E.S. Eco-friendly green synthesis of Ag@Fe bimetallic nanoparticles: Antioxidant, antimicrobial and photocatalytic degradation of bromothymol blue. *J. Photochem. Photobiol. B Biol.* **2018**, *185*, 143–152. [[CrossRef](#)] [[PubMed](#)]
58. Das, D.; Ghosh, R.; Mandal, P. Biogenic synthesis of silver nanoparticles using S1 genotype of *Morus alba* leaf extract: Characterization, antimicrobial and antioxidant potential assessment. *SN Appl. Sci.* **2019**, *1*, 498. [[CrossRef](#)]
59. de Castro, D.T.; do Nascimento, C.; Alves, O.L.; de Souza Santos, E.; Agnelli, J.A.M.; Dos Reis, A.C. Analysis of the oral microbiome on the surface of modified dental polymers. *Arch. Oral Biol.* **2018**, *93*, 107–114. [[CrossRef](#)]
60. Yin, I.X.; Zhang, J.; Zhao, I.S.; Mei, M.L.; Li, Q.; Chu, C.H. The antibacterial mechanism of silver nanoparticles and its application in dentistry. *Int. J. Nanomed.* **2020**, *15*, 2555–2562. [[CrossRef](#)]
61. Staats, K.; Pilz, M.; Sun, J.; Boiadjieva-Scherzer, T.; Kronberger, H.; Tobudic, S.; Windhager, R.; Holinka, J. Antimicrobial potential and osteoblastic cell growth on electrochemically modified titanium surfaces with nanotubes and selenium or silver incorporation. *Sci. Rep.* **2022**, *12*, 8298. [[CrossRef](#)]
62. Filipović, N.; Ušjak, D.; Milenković, M.T.; Zheng, K.; Liverani, L.; Boccaccini, A.R.; Stevanović, M.M. Comparative study of the antimicrobial activity of selenium nanoparticles with different surface chemistry and structure. *Front. Bioeng. Biotechnol.* **2021**, *8*, 624621. [[CrossRef](#)]
63. Boey, A.; Ho, H.K. All roads lead to the liver: Metal nanoparticles and their implications for liver health. *Small* **2020**, *16*, 2000153. [[CrossRef](#)] [[PubMed](#)]
64. Sinclair, T.R.; van den Hengel, S.K.; Raza, B.G.; Rutjes, S.A.; de Roda Husman, A.M.; Peijnenburg, W.J.; Roesink, H.E.D.; de Vos, W.M. Surface chemistry-dependent antiviral activity of silver nanoparticles. *Nanotechnology* **2021**, *32*, 365101. [[CrossRef](#)] [[PubMed](#)]

65. Rana, A.; Yadav, K.; Jagadevan, S. A comprehensive review on green synthesis of nature-inspired metal nanoparticles: Mechanism, application and toxicity. *J. Clean. Prod.* **2020**, *272*, 122880. [[CrossRef](#)]
66. Feng, X.; Chen, A.; Zhang, Y.; Wang, J.; Shao, L.; Wei, L. Central nervous system toxicity of metallic nanoparticles. *Int. J. Nanomed.* **2015**, *10*, 4321–4340.
67. Stankic, S.; Suman, S.; Haque, F.; Vidic, J. Pure and multi metal oxide nanoparticles: Synthesis, antibacterial and cytotoxic properties. *J. Nanobiotechnol.* **2016**, *14*, 73. [[CrossRef](#)] [[PubMed](#)]
68. Selim, Y.; Azb, M.; Ragab, I.; Abd El-Azim, M. Green synthesis of zinc oxide nanoparticles using aqueous extract of *Deverra tortuosa* and their cytotoxic activities. *Sci. Rep.* **2020**, *10*, 3445. [[CrossRef](#)]
69. Akter, M.; Sikder, M.T.; Rahman, M.M.; Ullah, A.A.; Hossain, K.F.B.; Banik, S.; Hosokawa, T.; Saito, T.; Kurasaki, M. A systematic review on silver nanoparticles-induced cytotoxicity: Physicochemical properties and perspectives. *J. Adv. Res.* **2018**, *9*, 1–16. [[CrossRef](#)]
70. Lewinski, N.; Colvin, V.; Drezek, R. Cytotoxicity of nanoparticles. *Small* **2008**, *4*, 26–49. [[CrossRef](#)]

Disclaimer/Publisher's Note: The statements, opinions and data contained in all publications are solely those of the individual author(s) and contributor(s) and not of MDPI and/or the editor(s). MDPI and/or the editor(s) disclaim responsibility for any injury to people or property resulting from any ideas, methods, instructions or products referred to in the content.